Computer Assisted Mechanics and Engineering Sciences, 9: 271–290, 2002.

A monotone predictor–corrector scheme for advection

Radosław Trębiński
Military Academy of Technology, ul. Kaliskiego 2, 00–908 Warsaw, Poland

(Received October 12, 2000)

A monotone predictor–corrector finite difference scheme solving the advection equation has been proposed. A geometrical interpretation of the Burstein scheme forms a basis for construction of the new scheme. The main idea consists in defining a proper limitation algorithm in the predictor step preventing formation of new extremes of the solution profile. Various variants of the scheme have been tested for the linear advection equation and an optimum version has been chosen for further developments. Extensions to the nonlinear case and inhomogenous, solution independent velocity field have been made. Application of the time splitting procedure enables the scheme to be applied for multidimensional advection problems. For chosen test problems the scheme behaves better than schemes proposed in the literature.

Keywords: finite difference schemes, monotone schemes, advection equation

1. Introduction

Over the last few decades a search has been continuing to devise finite difference schemes properly resolving sharp profiles of the solution of hyperbolic partial differential equations. The main problems to copy with are numerical diffusion and numerical dispersion. The first one blurs fine details of the solution. The second one generates spurious oscillations, considerably deforming solution profiles. The numerical diffusion and the numerical dispersion are in some way antagonists. It is very difficult to find a compromise between them. The traditional approach to this problem is to introduce artificial diffusion, which damps oscillations without causing large smearing of sharp profiles. This von Neumann and Richtmayer's idea [7] was being brought to perfection for years until new concepts were proposed. These concepts led to finite difference schemes that produce essentially no oscillations and cause only minor numerical diffusion. The name "monotone schemes" is often used in respect to them. It emphasizes a desirable property of the numerical solution consisting in preserving monotone profiles of numerically modeled discontinuities. As it was shown in [1], there is a principal difficulty to construct fully monotone schemes of order higher than the first for the solution of nonlinear equations. So the name "monotone" does not fully fit to many schemes considered as being monotone. The term "essentially nonoscillatory" introduced by Harten and Osher [6] would better fit. However, having in mind that the name "monotone" may mean "producing at most very small oscillations", we will use it further on.

Many monotone schemes have been proposed. FCT [2], TVD [9], MUSCL [11], ENO [6] and PPM [4] schemes belong to the most important. They have many modifications producing solutions having different properties. In the review paper by Young and Przekwas [12] the Roe and Sweby TVD and the Collela and Woodward PPM schemes were shown to produce the less deformed profiles of the solution of the nonlinear advection equation. In this paper solutions produced by these schemes are used as a reference for assessment of a new scheme.

The classical predictor–corrector Lax–Wendroff scheme, in the form proposed by Burstein [3], is a starting point for construction of a new monotone scheme for the advection equation. Geometrical interpretation of the Burstein scheme for the linear case makes the basis for a modification of the predictor step. Various algorithms for the predictor are analyzed. An algorithm producing the best results is generalized to the case of velocity field depending on the solution and changing both in space and time. Application to many dimensions is also considered.

2. Linear case

The Burstein scheme [3] for the advection equation

$$u_t + [F(u)]_x = 0 \tag{1}$$

has a form

- predictor

$$u_{i+1/2}^{n+1/2} = \frac{1}{2}(u_i^n + u_{i+1}^n) - \frac{1}{2}\lambda[F(u_{i+1}^n) - F(u_i^n)]\,, \qquad \lambda = h/\tau, \tag{2}$$

- corrector

$$u_i^{n+1} = u_i^n - \lambda[F(u_{i+1/2}^{n+1/2}) - F(u_{i-1/2}^{n+1/2})]\,, \tag{3}$$

where u_i^n denotes the value of the numerical solution at location x_i at time t^n, h and τ mean space and time steps of the grid.

Values of the solution calculated in predictor can be considered as some approximations of the solution at locations $x_{i+1/2} = (x_i + x_{i+1})/2$ at time $t^{n+1/2} = (t^n + t^{n+1})/2$. They can also be treated as some average values of the solution for $t \in [t^n\,,\, t^{n+1}]$ at the computational cells boundaries. Hence, $F(u_{i+1/2}^{n+1/2})$ can be considered as an average flux at a cell boundary.

In the case of homogenous, constant in time velocity field the flux can be expressed as $F(u) = au$, $a = \text{const}$. We assume provisionally that $a > 0$. Then we will generalize results for an arbitrary sign of velocity. The scheme (2)–(3) can be written in the form

- predictor

$$u_{i+1/2}^{n+1/2} = \frac{1}{2}(u_i^n + u_{i+1}^n) - \frac{1}{2}\nu(u_{i+1}^n - u_i^n)\,, \qquad \nu = a\lambda, \tag{4}$$

- corrector

$$u_i^{n+1} = u_i^n - \nu(u_{i+1/2}^{n+1/2} - u_{i-1/2}^{n+1/2})\,. \tag{5}$$

The predictor step (4) can be interpreted as a linear interpolation formula between values of the solution at nodes i and $i+1$ at time t^n. An approximate value of the solution at point $x = x_{i+1/2} - a\tau/2$, $t = t^n$ is determined. It is a starting point of a characteristic line coming at the cell boundary at time $t^{n+1/2}$ – Fig. 1.

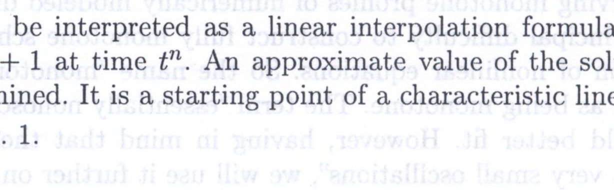

Fig. 1. Illustration for the geometrical interpretation of the formula (4)

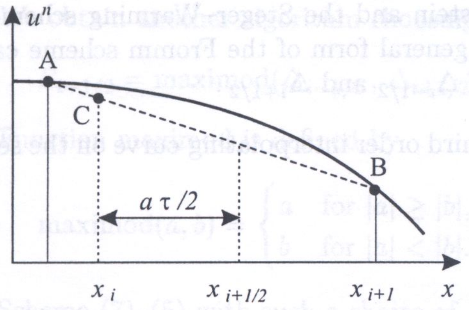

Fig. 2. Geometrical interpretation of the predictor step of the Burstein scheme

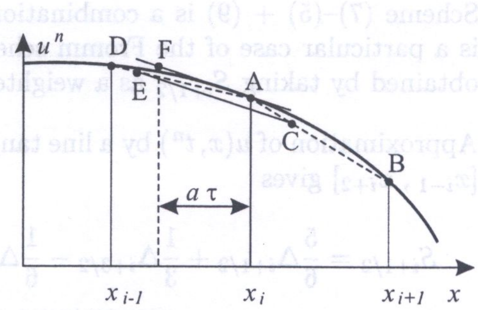

Fig. 3. Geometrical interpretation of the corrector step of the Burstein scheme

A geometric interpretation of Eq. (4) is given in Fig. 2. The solid line is a continuous representation of the solution $u^n(x) \equiv u(x, t^n)$. At the section $[x^i\,, x^{i+1}]$ the function $u^n(x)$ is approximated by a straight line AB. The point C corresponds to the approximate value of the solution determined at the predictor step $u^{n+1/2}_{i+1/2}$.

Figure 3 shows a geometric interpretation of the corrector step. The points D, A, B correspond to $u^n_{i-1}\,, u^n_i\,, u^n_{i+1}$. The points C and E represent solution determined in the predictor step. We join these points by a straight line and then we construct a line starting at point A and parallel to the line CE. The point F lying on that line in a distance $a\tau$ from the node i represents solution determined in the corrector. It can be shown that the point F lies on a parabola joining points D, A and B. Hence, a sequence of two linear interpolations is equivalent to the interpolation by a parabola.

Defining a symbol

$$S_{i+1/2} \equiv \Delta_{i+1/2} \equiv u^n_{i+1} - u^n_i\,, \tag{6}$$

we can write down the predictor step in the form

$$u^{n+1/2}_{i+1/2} = u^n_i + \frac{1}{2}(1-\nu)S_{i+1/2}\,. \tag{7}$$

Modification of the predictor step will consist in application of an algorithm for the determining of $S_{i+1/2}$. The algorithm will be based on construction of various approximations of the function $u(x, t^n)$ in the vicinity of the node i. The following approximations will be considered.

S0. The simplest approximation is $u^{n+1/2}_{i+1/2} = u^n_i$ ($S_{i+1/2} = 0$). Then the scheme (4)–(5) becomes equivalent to the up-wind scheme.

S1. In the Burstein scheme $u(x, t^n)$ in the vicinity of the node i is approximated by a secant line joining points corresponding to u^n_i and u^n_{i+1}. $S_{i+1/2}$ is given by (6).

S2. $u(x, t^n)$ can be approximated by a secant line at the section $[x_{i-1}\,, x_i]$. Then

$$S_{i+1/2} = \Delta_{i-1/2}\,. \tag{8}$$

The scheme (7)–(5) becomes equivalent to the second order up-wind scheme (the Steger–Warming scheme).

S3. $u(x, t^n)$ can be approximated by a line tangent at $x = x_i$ to a parabola constructed on the basis of $u^n_{i-1}\,, u^n_i\,, u^n_{i+1}$ values. In this case

$$S_{i+1/2} = \frac{1}{2}(u^n_{i+1} - u^n_{i-1}) = \frac{1}{2}(\Delta_{i-1/2} + \Delta_{i+1/2})\,. \tag{9}$$

Scheme (7)–(5) + (9) is a combination of the Burstein and the Steger–Warming schemes. It is a particular case of the Fromm scheme [5]. The general form of the Fromm scheme can be obtained by taking $S_{i+1/2}$ as a weighted average of $\Delta_{i-1/2}$ and $\Delta_{i+1/2}$.

S4. Approximation of $u(x, t^n)$ by a line tangent to the third order interpolating curve on the section $[x_{i-1}, x_{i+2}]$ gives

$$S_{i+1/2} = \frac{5}{6}\Delta_{i+1/2} + \frac{1}{3}\Delta_{i+3/2} - \frac{1}{6}\Delta_{i-1/2}. \tag{10}$$

S5. Interpolating $u(x, t^n)$ on the section $[x_{i-2}, x_{i+2}]$ by the fourth order polynomial and approximating the function by a line tangent at $x = x_i$ to the interpolation curve leads to the following expression

$$S_{i+1/2} = \frac{2}{3}(u^n_{i+1} - u^n_{i-1}) - \frac{1}{12}(u^n_{i+2} - u^n_{i-2}). \tag{11}$$

S6. Approximation of $u(x, t^n)$ for $x \in [x_{i-1}, x_{i+1}]$ by a parabola expresses $S_{i+1/2}$ as a function of the Courant number ν

$$S_{i+1/2} = \frac{1}{4}[3\Delta_{i+1/2} + \Delta_{i-1/2} - \nu(\Delta_{i+1/2} - \Delta_{i-1/2})]. \tag{12}$$

Scheme (7)–(5) is in this case of the third order of approximation and it corresponds to the cubic interpolation at the section $[x_{i-2}, x_{i+1}]$. On the strength of the Strang theorem [8] the scheme is stable for $\nu \in [0, 1]$.

S7. Approximation of $u(x, t^n)$ for $x \in [x_{i-1}, x_{i+2}]$ by the third order interpolation polynomial gives

$$S_{i+1/2} = \Delta_{i+1/2} - \frac{1}{8}(\Delta_{i+3/2} - \Delta_{i-1/2}) - \frac{1}{12}\nu(\Delta_{i+3/2} - 2\Delta_{i-1/2} + \Delta_{i+1/2})$$
$$+ \frac{1}{24}\nu^2(\Delta_{i+3/2} - 2\Delta_{i+1/2} + \Delta_{i-1/2}). \tag{13}$$

Scheme (7)–(5) is in this case of the fourth order of approximation and it corresponds to the fourth order interpolation at the section $[x_{i-2}, x_{i+2}]$. On the strength of the Strang theorem the scheme is stable for $\nu \in [0, 1]$.

S8. $u(x, t^n)$ in the vicinity of the node i can be approximated by the secant line for $x \in [x_{i-1}, x_i]$ or by the secant line for $x \in [x_i, x_{i+1}]$ depending on relation between slopes of these lines. If we choose the one having the less slope we obtain

$$S_{i+1/2} = \operatorname{minimod}(\Delta_{i-1/2}, \Delta_{i+1/2}). \tag{14}$$

Function minimod is defined by

$$\operatorname{minimod}(a, b) = \begin{cases} a & \text{for } |a| \le |b|, \\ b & \text{for } |a| > |b|. \end{cases} \tag{15}$$

If we add an additional condition

$$S_{i+1/2} = 0 \qquad \text{if } \Delta_{i-1/2}\Delta_{i+1/2} < 0, \tag{16}$$

the scheme (7)–(5) becomes equivalent to the Van Leer MUSCL scheme [11].

S9. We obtain another algorithm choosing

$$S_{i+1/2} = \text{maximod}(\Delta_{i-1/2}\,,\, \Delta_{i+1/2})\,. \tag{17}$$

Function maximod is defined by

$$\text{maximod}(a, b) = \begin{cases} a & \text{for } |a| \geq |b|, \\ b & \text{for } |a| < |b|. \end{cases} \tag{18}$$

Scheme (7)–(5) with such a choice of $S_{i+1/2}$ has no counterparts.

S10. Similarly to the preceding approximation we can calculate $S_{i+1/2}$ on the basis of two parabolas interpolating $u(x, t^n)$ for $x \in [x_{i-2}\,,\, x_i]$ and $x \in [x_i\,,\, x_{i+2}]$

$$\begin{aligned} &S_{i+1/2} = \text{maximod}(D_{i-1/2}\,,\, D_{i+1/2})\,, \\ &D_{i+1/2} = 5\Delta_{i+1/2} - \Delta_{i+3/2} - \nu(\Delta_{i+3/2} - \Delta_{i+1/2})\,. \end{aligned} \tag{19}$$

The scheme defined in this way corresponds to a local switching between two third order schemes determined for $x \in [x_{i-3}\,,\, x_i]$ and $x \in [x_{i-1}\,,\, x_{i+2}]$. On the strength of the Strang theorem both schemes are unstable for $\nu \in (0, 1)$.

Above algorithms for calculation of $S_{i+1/2}$ define various schemes. Only S0 and S8 schemes are monotone. Others produce oscillations and S10 is unstable. In order to make them monotone a limiting of the $S_{i+1/2}$ value is necessary. We will derive some limiting conditions basing on the demand that the value of u_i^{n+1} is contained between u_{i-1}^n and u_i^n values. When this demand is fulfilled no additional extremes can arise at t^{n+1} that are not present at t^n.

Let us consider first a profile of $u(x, t^n)$ shown in Fig. 4. Points A_i and A_{i-1} correspond to u_i^n and u_{i-1}^n, while points P_i and P_{i+1} to $u_{i-1/2}^{n+1/2}$ and $u_{i+1/2}^{n+1/2}$. The point C_i represents the solution obtained in the corrector step. When C_i is above A_{i-1}, a new maximum may form. In order to avoid this the following relation should be fulfilled

$$u_i^{n+1} \leq u_{i-1}^n\,. \tag{20}$$

Making use of (5) and (7) we obtain

$$u_i^n - \nu\left[u_i^n + \frac{1}{2}(1-\nu)S_{i+1/2} - u_{i-1}^n - \frac{1}{2}(1-\nu)S_{i-1/2}\right] \leq u_{i-1}^n \tag{21}$$

and

$$S_{i+1/2} \geq \frac{1}{2}\nu^{-1}\Delta_{i-1/2} + S_{i-1/2}\,. \tag{22}$$

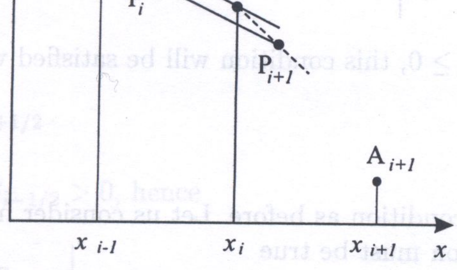

Fig. 4. Illustration for the limitation method of S, the case $\Delta_{i+1/2} < \Delta_{i-1/2} < 0$

We assume that $S_{i+1/2}$ have the same sign as $\Delta_{i+1/2}$. In the area, where the solution is monotone, this assumption is true. It may be violated only near extremes. In order to prevent this we include the condition (16). In further considerations we will assume this protection to be active.

For the considered profile $S_{i+1/2} < 0$, hence

$$|S_{i+1/2}| \leq \left| \frac{1}{2}\nu^{-1}\Delta_{i-1/2} + S_{i-1/2} \right| . \tag{23}$$

Since $\Delta_{i-1/2} < 0$ and $S_{i-1/2} \leq 0$ this condition will be satisfied when

$$|S_{i+1/2}| \leq \frac{1}{2}\nu^{-1}\delta_{i-1/2}\,, \qquad \delta_{i-1/2} \equiv |\Delta_{i-1/2}|\,. \tag{24}$$

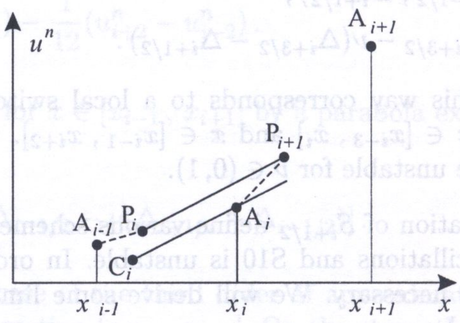

Fig. 5. Illustration for the limitation method of S, the case $\Delta_{i+1/2} > \Delta_{i-1/2} > 0$

Let us consider now the profile shown in Fig. 5. A new minimum may appear when C_i is below A_{i-1}. Therefore, the following relation must be true

$$u_i^{n+1} \geq u_{i-1}^n\,. \tag{25}$$

Making use of (5) and (7) we come to

$$u_i^n - \nu\left[u_i^n + \frac{1}{2}(1-\nu)S_{i+1/2} - u_{i-1}^n - \frac{1}{2}(1-\nu)S_{i-1/2}\right] \geq u_{i-1}^n \tag{26}$$

and

$$S_{i+1/2} \leq \frac{1}{2}\nu^{-1}\Delta_{i-1/2} + S_{i-1/2}\,. \tag{27}$$

For the considered profile $S_{i+1/2} > 0$, hence

$$|S_{i+1/2}| \leq \left| \frac{1}{2}\nu^{-1}\Delta_{i-1/2} + S_{i-1/2} \right| . \tag{28}$$

Because $\Delta_{i-1/2} > 0$ and $S_{i-1/2} \geq 0$, this condition will be satisfied when

$$|S_{i+1/2}| \leq \frac{1}{2}\nu^{-1}\delta_{i-1/2}\,. \tag{29}$$

We have come to the same condition as before. Let us consider now the profile shown in Fig. 6. In this case the following relation must be true

$$u_i^{n+1} \geq u_i^n\,. \tag{30}$$

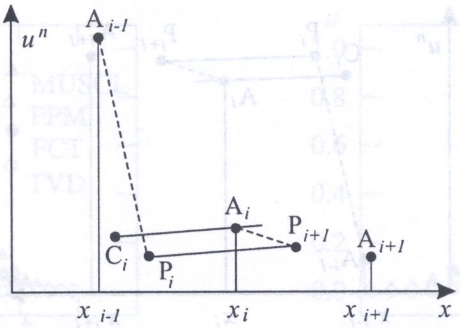

Fig. 6. Illustration for the limitation method of S, the case $\Delta_{i-1/2} < \Delta_{i+1/2} < 0$

So we have

$$u_i^n - \nu\left[u_i^n + \frac{1}{2}(1-\nu)S_{i+1/2} - u_{i-1}^n - \frac{1}{2}(1-\nu)S_{i-1/2}\right] \geq u_i^n \tag{31}$$

and

$$S_{i-1/2} \geq \frac{2}{1-\nu}\Delta_{i-1/2} + S_{i+1/2}\,. \tag{32}$$

For the considered profile $S_{i+1/2} < 0$. Therefore, it follows from (32)

$$|S_{i-1/2}| \leq \left|\frac{2}{1-\nu}\Delta_{i-1/2} + S_{i+1/2}\right|. \tag{33}$$

Because $\Delta_{i-1/2} < 0$ and $S_{i+1/2} \leq 0$, this condition is satisfied when

$$|S_{i-1/2}| \leq \frac{2}{1-\nu}\delta_{i-1/2}\,. \tag{34}$$

Increasing i by 1 we come to

$$|S_{i+1/2}| \leq \frac{2}{1-\nu}\delta_{i+1/2}\,. \tag{35}$$

The last considered profile is shown in Fig. 7. Monotone profile is preserved when

$$u_i^{n+1} \leq u_i^n\,. \tag{36}$$

This condition can be transformed to

$$u_i^n - \nu\left[u_i^n + \frac{1}{2}(1-\nu)S_{i+1/2} - u_{i-1}^n - \frac{1}{2}(1-\nu)S_{i-1/2}\right] \leq u_i^n \tag{37}$$

and

$$S_{i-1/2} \leq \frac{2}{1-\nu}\Delta_{i-1/2} + S_{i+1/2}\,. \tag{38}$$

For the considered profile $S_{i-1/2} > 0$, hence

$$|S_{i-1/2}| \leq \left|\frac{2}{1-\nu}\Delta_{i-1/2} + S_{i+1/2}\right|. \tag{39}$$

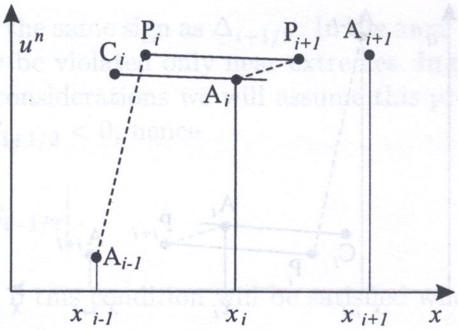

Fig. 7. Illustration for the limitation method of S, the case $\Delta_{i-1/2} > \Delta_{i+1/2} > 0$

Since $\Delta_{i-1/2} > 0$ and $S_{i+1/2} \geq 0$, we come to

$$|S_{i-1/2}| \leq \frac{2}{1-\nu}\delta_{i-1/2}\,. \tag{40}$$

Increasing i by 1 we come again to the condition (35).

Let us observe that a common feature of profiles shown in Figs. 4 and 5 is that $\delta_{i+1/2} > \delta_{i-1/2}$ while in the case of profiles shown in Figs. 6 and 7 $\delta_{i+1/2} < \delta_{i-1/2}$. Taking it into account we can propose the following algorithm for limiting the $S_{i+1/2}$ value

$$\begin{aligned} S^c_{i+1/2} &= \begin{cases} 0 & \text{if } \Delta_{i-1/2}\Delta_{i+1/2} < 0, \\ S_a & \text{if } \Delta_{i-1/2}\Delta_{i+1/2} \geq 0, \end{cases} \\ S_a &= \begin{cases} \text{minimod}\left(S_{i+1/2}\,,\, \frac{2}{\nu}\Delta_{i-1/2}\right) & \text{if } \delta_{i+1/2} \geq \delta_{i-1/2}\,, \\ \text{minimod}\left(S_{i+1/2}\,,\, \frac{2}{1-\nu}\Delta_{i+1/2}\right) & \text{if } \delta_{i+1/2} < \delta_{i-1/2}\,, \end{cases} \end{aligned} \tag{41}$$

$S^c_{i+1/2}$ means the corrected value of $S_{i+1/2}$.

The following test problems will be used for evaluation of the schemes S1–S10 used with the limiting algorithm (41)

$$\begin{aligned} &u_t + au_x = 0, \qquad a = 1 \\ &u(x,0) = \varphi(x), \qquad x \in [0,100] \\ &u(0,t) = u(100,t) \end{aligned} \tag{42}$$

The function $\varphi(x)$ is defined as

- square wave test

$$\varphi(x) = \begin{cases} 1 & \text{for } x \in [10,20], \\ 0 & \text{for } x \notin [10,20], \end{cases} \tag{43}$$

- blast wave test

$$\varphi(x) = \begin{cases} (x/10-1)^5 & \text{for } x \in [10,20], \\ 0 & \text{for } x \notin [10,20], \end{cases} \tag{44}$$

- Gaussian test

$$\varphi(x) = \exp[-(x-15.5)^2/2.773]. \tag{45}$$

In all calculations $h = 1$, $\nu = 0.5$.

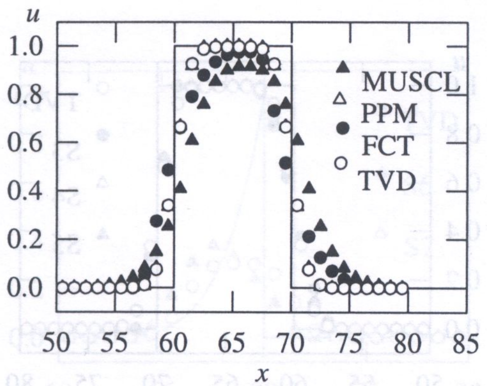

Fig. 8. Results of the square wave test for FCT, TVD, MUSCL and PPM schemes

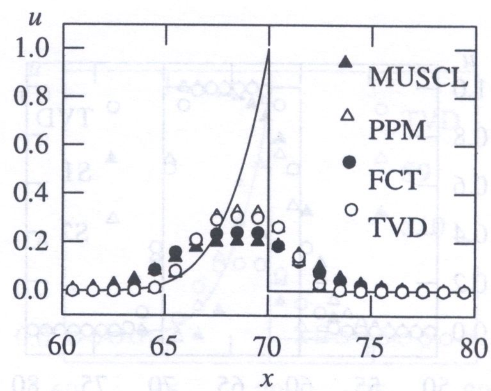

Fig. 9. Results of the blast wave test for FCT, TVD, MUSCL and PPM schemes

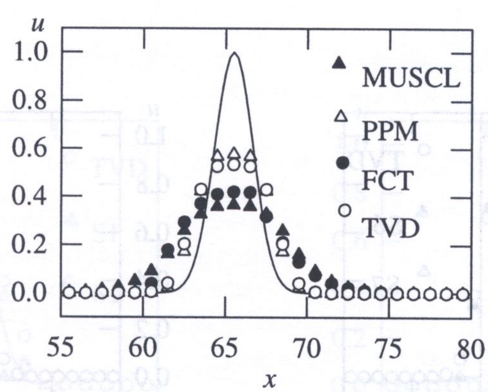

Fig. 10. Results of the Gaussian test for FCT, TVD, MUSCL and PPM schemes

The exact solution for $t = 50$ (100 time steps) for different $\varphi(x)$ is shown in Figs. 8–10. Results obtained by FCT, MUSCL, TVD and PPM schemes are also shown. In accordance with the inferences drawn in [12] the TVD and PPM schemes produce the less deformation of the solution. Results of the TVD scheme are used as a reference in evaluation of analyzed schemes – Figs. 11–22.

All the tests have proven that the algorithm (41) preserves monotone profiles. S9 and S10 schemes produce numerical solution closer to the exact solution than that obtained by the use of the TVD scheme. The S10 scheme shows the less numerical diffusion. However, it compresses too much some profiles. This effect is pronounced for the "blast wave test" – Fig. 18. Finally, the S9 scheme was chosen for further considerations. The acronym PCM (predictor–corrector–monotone) will be used in respect to it.

Let us consider the case $a < 0$. The predictor step has a form

$$u_{i+1/2}^{n+1/2} = u_{i+1}^{n} - \frac{1}{2}(1-\nu)S_{i+1/2}, \quad \nu = |a|\,\Delta t/\Delta x \tag{46}$$

Repeating analysis made for $a > 0$, we come to the following conditions limiting $S_{i+1/2}$

$$\begin{aligned} S_{i+1/2}^{c} &= \begin{cases} 0 & \text{if } \Delta_{i+1/2}\Delta_{i+3/2} < 0, \\ S_a & \text{if } \Delta_{i+1/2}\Delta_{i+3/2} \geq 0, \end{cases} \\ S_a &= \begin{cases} \text{minimod}\left(S_{i+1/2}\,,\ \frac{2}{\nu}\Delta_{i+1/2}\right) & \text{if } \delta_{i+1/2} \geq \delta_{i+3/2}\,, \\ \text{minimod}\left(S_{i+1/2}\,,\ \frac{2}{1-\nu}\Delta_{i+1/2}\right) & \text{if } \delta_{i+1/2} < \delta_{i+3/2}\,. \end{cases} \end{aligned} \tag{47}$$

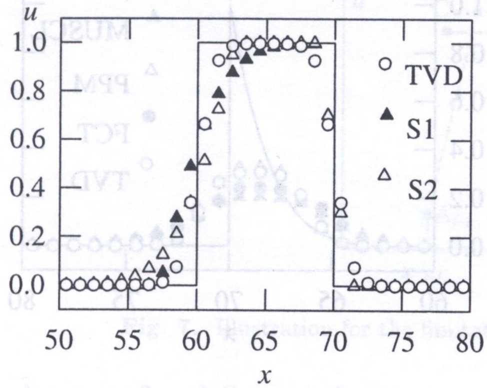

Fig. 11. Results of the square wave test for S1, S2 and TVD schemes

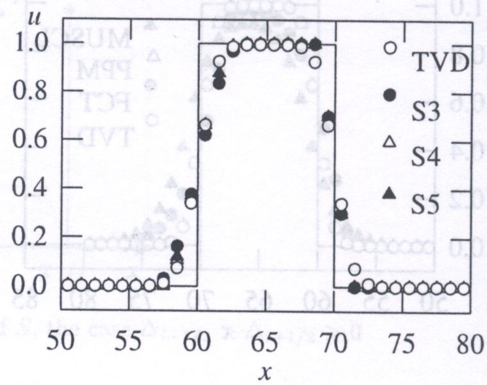

Fig. 12. Results of the square wave test for S3, S4, S5 and TVD schemes

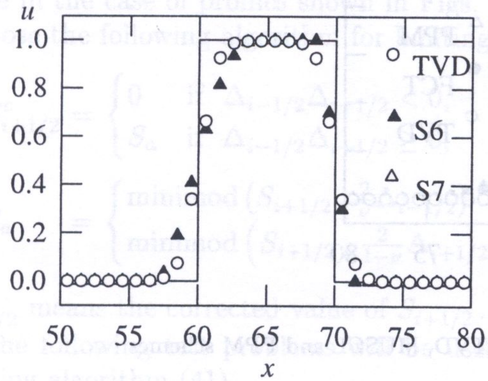

Fig. 13. Results of the square wave test for S6, S7 and TVD schemes

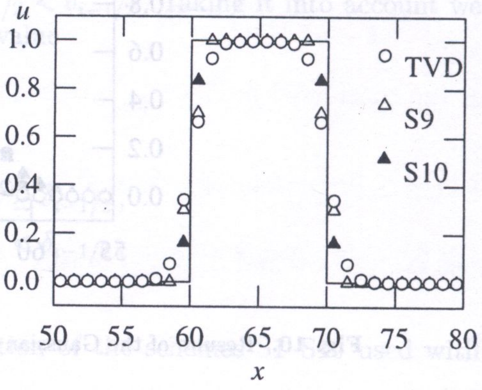

Fig. 14. Results of the square wave test for S9, S10 and TVD schemes

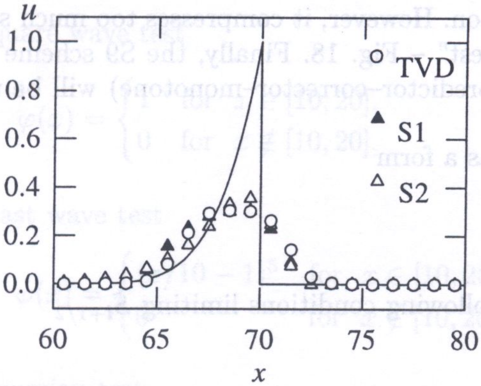

Fig. 15. Results of the blast wave test for S1, S2 and TVD schemes

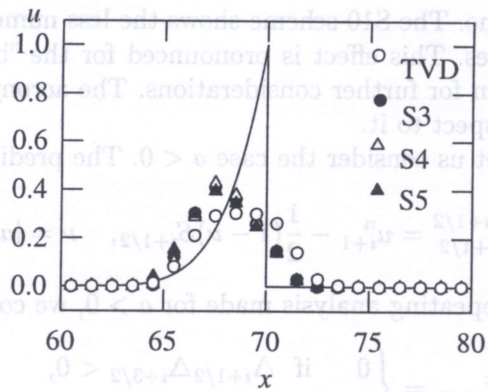

Fig. 16. Results of the blast wave test for S3, S4, S5 and TVD schemes

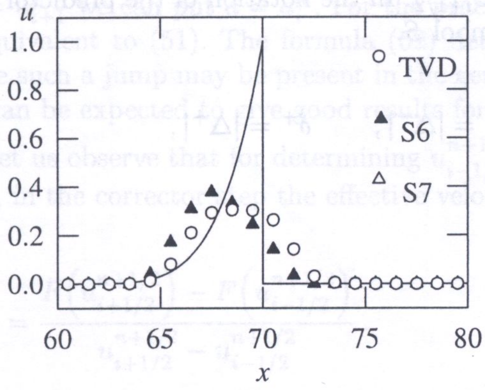

Fig. 17. Results of the blast wave test for S6, S7 and TVD schemes

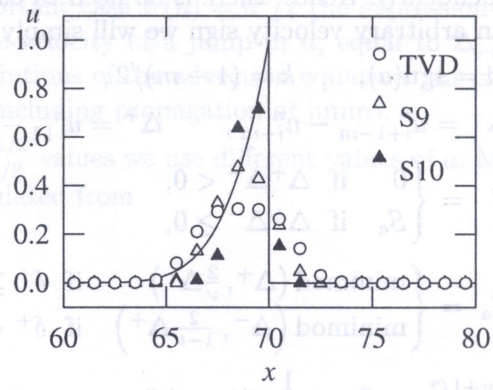

Fig. 18. Results of the blast wave test for S9, S10 and TVD schemes

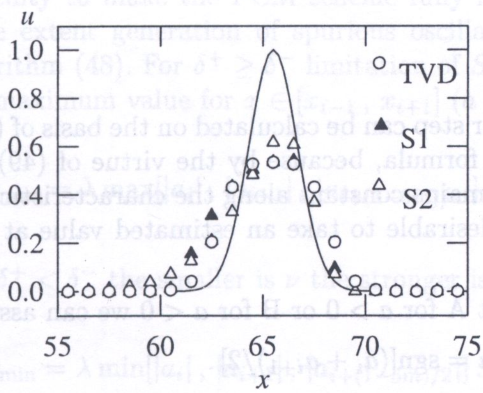

Fig. 19. Results of the Gaussian test for S1, S2 and TVD schemes

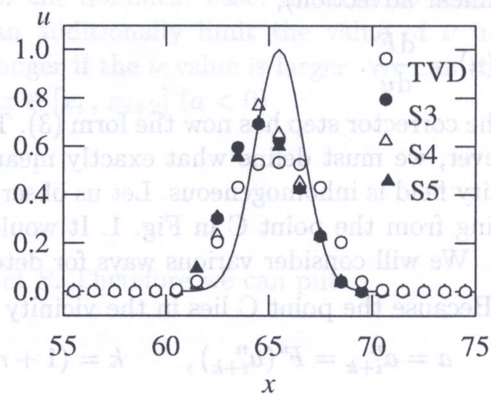

Fig. 20. Results of the Gaussian test for S3, S4, S5 and TVD schemes

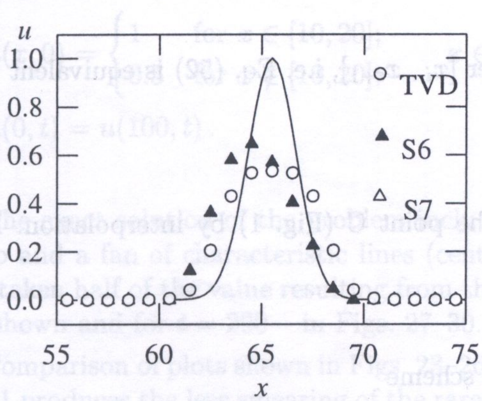

Fig. 21. Results of the Gaussian test for S6, S7 and TVD schemes

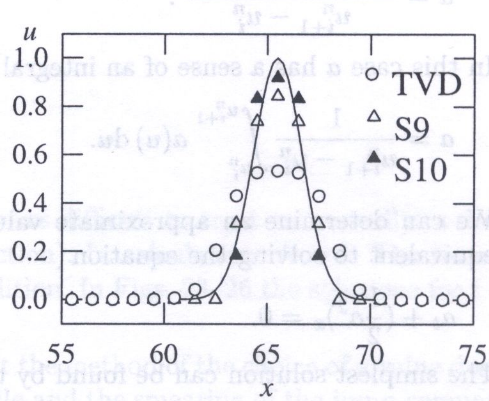

Fig. 22. Results of the Gaussian test for S9, S10 and TVD schemes

Let us observe, that the algorithm for the correction of $S_{i+1/2}$ values is local, i.e. they are limited independently. Hence, there is no need to use an array $S_{i+1/2}$. In the notation of the predictor step for an arbitrary velocity sign we will simply use the symbol S.

$$
\begin{aligned}
&m = \operatorname{sgn}(a), \qquad k = (1-m)/2, \\
&\Delta^- = u^n_{i+1-m} - u^n_{i-m}, \qquad \Delta^+ = u^n_{i+1} - u^n_i, \qquad \delta^- = |\Delta^-|, \qquad \delta^+ = |\Delta^+|, \\
&S = \begin{cases} 0 & \text{if } \Delta^+\Delta^- < 0, \\ S_a & \text{if } \Delta^+\Delta^- \geq 0, \end{cases} \\
&S_a = \begin{cases} \operatorname{minimod}\left(\Delta^+, \frac{2}{\nu}\Delta^-\right) & \text{if } \delta^+ \geq \delta^-, \\ \operatorname{minimod}\left(\Delta^-, \frac{2}{1-\nu}\Delta^+\right) & \text{if } \delta^+ < \delta^-, \end{cases} \\
&u^{n+1/2}_{i+1/2} = u^n_{i+k} + \frac{1}{2} m(1-\nu)S.
\end{aligned}
\tag{48}
$$

3. Nonlinear case

We will try to generalize the PCM scheme to the case of the velocity field depending on the solution (nonlinear advection),

$$
a(u) = \frac{\mathrm{d}F}{\mathrm{d}u}\,. \tag{49}
$$

The corrector step has now the form (3). The predictor step can be calculated on the basis of (48). However, we must define what exactly means a in this formula, because by the virtue of (49) the velocity field is inhomogeneous. Let us observe that a remains constant along the characteristic line starting from the point C in Fig. 1. It would be then desirable to take an estimated value at this point. We will consider various ways for determining a.

A1. Because the point C lies in the vicinity of the point A for $a > 0$ or B for $a < 0$ we can assume

$$
a = a^n_{i+k} = F'(u^n_{i+k})\,, \qquad k = (1+m)/2, \qquad m = \operatorname{sgn}[(a_i + a_{i+1})/2]\,. \tag{50}
$$

A2. We can approximate a as an average for $x \in [x_i\,,\, x_{i+1}]$

$$
a = (a^n_i + a^n_{i+1})/2. \tag{51}
$$

A3. The form of the predictor step of the Burstein scheme (2) suggests that we can put

$$
a = \frac{F(u^n_{i+1}) - F(u^n_i)}{u^n_{i+1} - u^n_i}\,. \tag{52}
$$

In this case a has a sense of an integral average over $[x_i\,,\, x_{i+1}]$, i.e. Eq. (52) is equivalent to

$$
a = \frac{1}{u^n_{i+1} - u^n_i} \int_{u^n_i}^{u^n_{i+1}} a(u)\,\mathrm{d}u. \tag{53}
$$

A4. We can determine an approximate value of a at the point C (Fig. 1) by interpolation. It is equivalent to solving the equation

$$
a_t + \left(\frac{1}{2}a^2\right)_x = 0. \tag{54}
$$

The simplest solution can be found by the up-wind scheme

$$
a = (a_i + a_{i+1})/2, \qquad S = a_{i+1} - a_i\,, \qquad a = a_i + \frac{1}{2}(1 - \lambda a)S. \tag{55}
$$

A5. The solution of (54) can be found by the PCM scheme with the choice of a in (48) given by (51).

The formula (52) can be treated as a finite difference approximation of (49). Therefore, for $u_i^n = u_{i+1}^n$ we can put $a = a_i^n$. For the practically important case $F(u) = u^2/2$ the expression (52) is equivalent to (51). The formula (52) determines the velocity of a jump in u, equal to $\Delta_{i+1/2}$. Since such a jump may be present in the generalized solutions of the advection equation, the choice A3 can be expected to give good results for problems including propagation of jumps.

Let us observe that for determining $u_{i-1/2}^{n+1/2}$ and $u_{i+1/2}^{n+1/2}$ values we use different values of a. Moreover, in the corrector step the effective velocity is calculated from

$$a = \frac{F\left(u_{i+1/2}^{n+1/2}\right) - F\left(u_{i-1/2}^{n+1/2}\right)}{u_{i+1/2}^{n+1/2} - u_{i-1/2}^{n+1/2}}. \tag{56}$$

As a result, the scheme for the nonlinear case does not correspond fully to the interpolation procedure described for the linear case. In the aftermath of this the limiting algorithm (48) may not preserve monotone profiles. On the other hand, if we chose the same velocity for determining $u_{i-1/2}^{n+1/2}$, $u_{i+1/2}^{n+1/2}$ and u_i^n we would obtain a nonconservative scheme. As we can see, there is a principal difficulty to make the PCM scheme fully monotone for the nonlinear case. In order to reduce in some extent generation of spurious oscillations we can additionally limit the value of ν in the algorithm (48). For $\delta^+ \geq \delta^-$ limitation of S will be stronger if the ν value is larger. We can choose the maximum value for $x \in [x_{i-1}, x_{i+1}]$ $(a > 0)$ or for $x \in [x_i, x_{i+2}]$ $(a < 0)$

$$\nu_{\max} = \lambda \max[|a_i|, |a_{i+1}|, |a_{i+(1-3m)/2}|]. \tag{57}$$

For $\delta^+ < \delta^-$ the smaller is ν the stronger is limitation of S. Therefore we can put

$$\nu_{\min} = \lambda \min[|a_i|, |a_{i+1}|, |a_{i+(1-3m)/2}|]. \tag{58}$$

Schemes based on different choice of a value have been tested for the following problem

$$\begin{aligned} & u_t + \left(\frac{2}{3}u^{1.5}\right)_x = 0, \\ & u(x,0) = \begin{cases} 1 & \text{for } x \in [10,20]; \\ 0.5 & \text{for } x \notin [10,20]; \end{cases} \qquad x \in [0,100], \\ & u(0,t) = u(100,t). \end{aligned} \tag{59}$$

The exact solution of the problem includes two features difficult to treat numerically: a moving jump and a fan of characteristic lines (centered rarefaction). In calculations $h = 1$. The time step was taken half of the value resulting from the CFL condition. In Figs. 23–26 the solutions for $t = 50$ are shown and for $t = 200$ – in Figs. 27–30.

Comparison of plots shown in Figs. 23–26 proves, that the method of the choice of a value denoted as A1 produces the less smearing of the rarefaction profile and the smearing of the jump comparable to other methods. The methods A2–A4 cause a small overshot (within 1% of the jump height), while no violation of monotone profile is observed for A1 and A5. For $t = 200$ all the methods give almost the same results. The position of jump is perfectly tracked. It is a consequence of the conservative form of the corrector step.

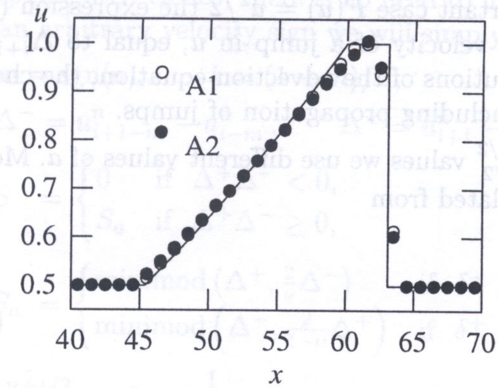

Fig. 23. Results of the square wave test in the nonlinear case for A1 and A2 methods of determining a; $t = 50$

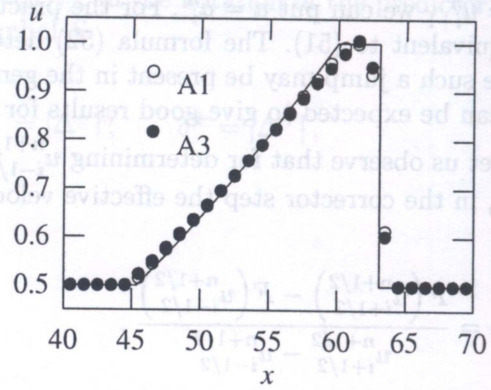

Fig. 24. Results of the square wave test in the nonlinear case for A1 and A3 methods of determining a; $t = 50$

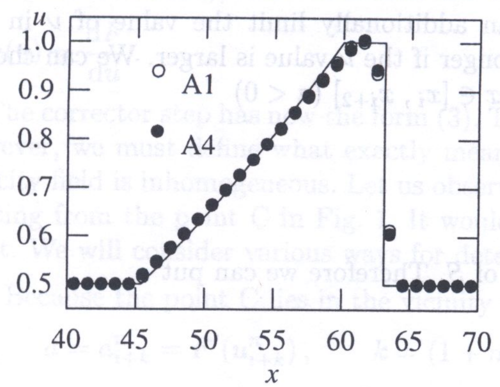

Fig. 25. Results of the square wave test in the nonlinear case for A1 and A4 methods of determining a; $t = 50$

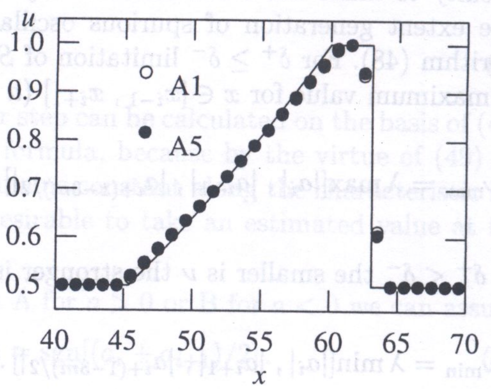

Fig. 26. Results of the square wave test in the nonlinear case for A1 and A5 methods of determining a; $t = 50$

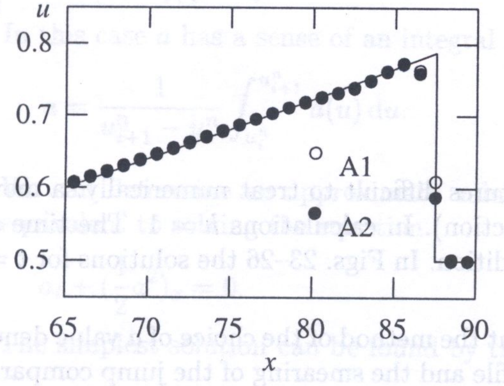

Fig. 27. Results of the square wave test in the nonlinear case for A1 and A2 methods of determining a; $t = 200$

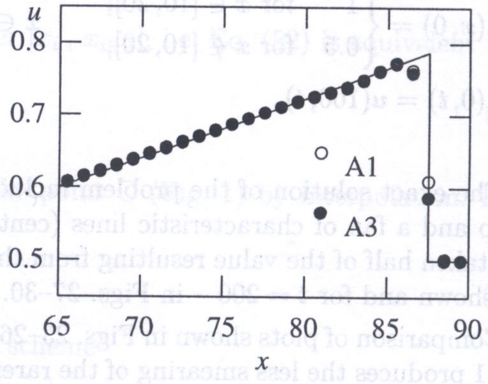

Fig. 28. Results of the square wave test in the nonlinear case for A1 and A3 methods of determining a; $t = 200$

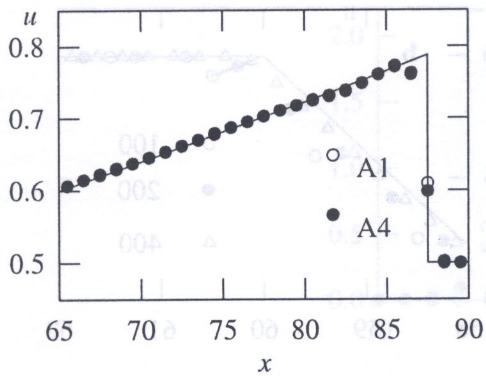

Fig. 29. Results of the square wave test in the nonlinear case for A1 and A4 methods of determining a; $t = 200$

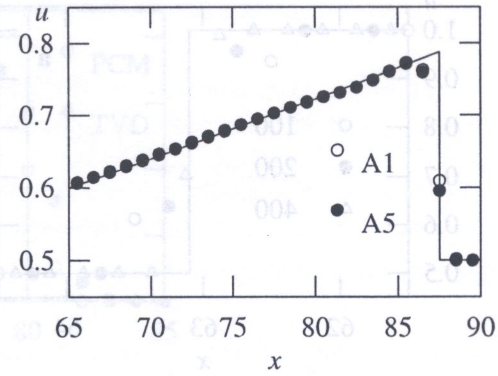

Fig. 30. Results of the square wave test in the nonlinear case for A1 and A5 methods of determining a; $t = 200$

Test results indicate the methods A1 and A5 as the best. Due to its simplicity the method A1 seems to be a rational choice. Therefore, the algorithm of the predictor step of the PCM scheme can be written in the form

$$
\begin{aligned}
&a = (a_i^n + a_{i+1}^n)/2, \qquad m = \operatorname{sgn}(a), \qquad k = (1-m)/2, \qquad a = a_{i+k}^n, \qquad \nu = \lambda|a|,\\
&\nu_{\max} = \lambda \max[|a_i^n|,\ |a_{i+1}^n|,\ |a_{i+(1-3m)/2}^n|],\\
&\nu_{\min} = \lambda \min[|a_i^n|,\ |a_{i+1}^n|,\ |a_{i+(1-3m)/2}^n|],\\
&\Delta^- = u_{i+1-m}^n - u_{i-m}^n, \qquad \Delta^+ = u_{i+1}^n - u_i^n, \qquad \delta^- = |\Delta^-|, \qquad \delta^+ = |\Delta^+|\\
&S \;=\; \begin{cases} 0 & \text{if } \Delta^+\Delta^- < 0,\\ S_a & \text{if } \Delta^+\Delta^- \geq 0,\end{cases}\\
&S_a \;=\; \begin{cases} \operatorname{minimod}\left(\Delta^+, \frac{2}{\nu_{\max}}\Delta^-\right) & \text{if } \delta^+ \geq \delta^-,\\ \operatorname{minimod}\left(\Delta^-, \frac{2}{1-\nu_{\min}}\Delta^+\right) & \text{if } \delta^+ < \delta^-,\end{cases}\\
&u_{i+1/2}^{n+1/2} = u_{i+k}^n + \frac{1}{2}m(1-\nu)S.
\end{aligned}
\tag{60}
$$

Results obtained for the PCM scheme defined by (60) are compared in Figs. 31 and 32 with results obtained by the use of the TVD and PPM schemes. The PCM scheme produces the least deformation of the solution profile.

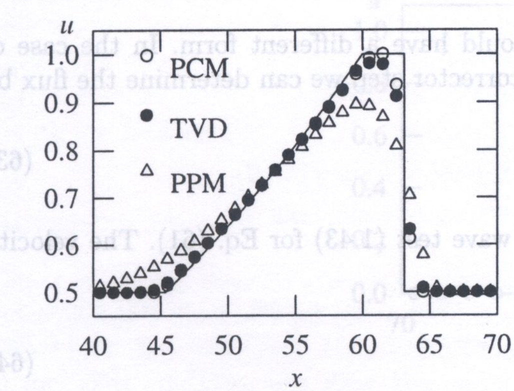

Fig. 31. Results of the square wave test in the nonlinear case for the PCM(A1), TVD and PPM schemes; $t = 50$

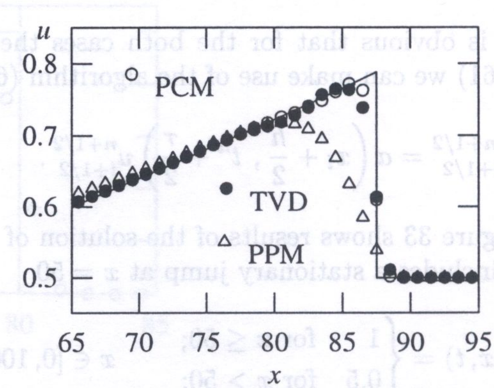

Fig. 32. Results of the square wave test in the nonlinear case for the PCM(A1), TVD and PPM schemes; $t = 200$

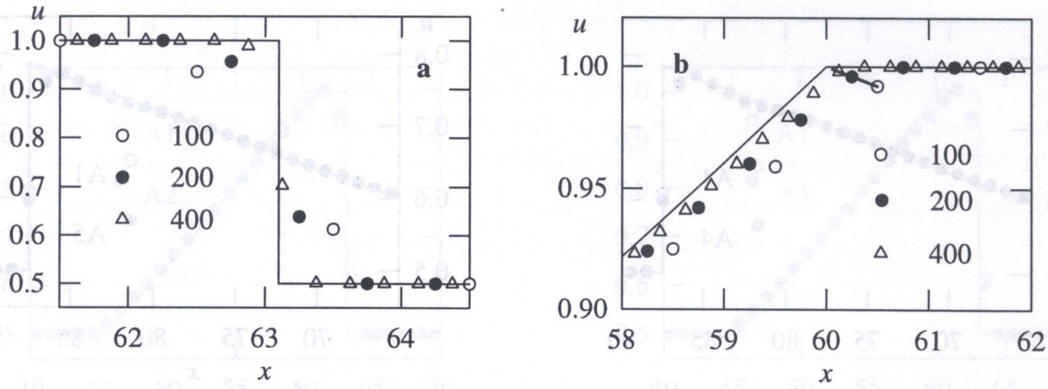

Fig. 33. The effects of the grid refinement (numbers of spatial steps are given) on the numerical solution in the vicinity of the strong (a) and weak (b) discontinuity

The PCM scheme is a second order scheme in the areas of the smooth solution. In the vicinity of strong discontinuities results obtained by the PCM scheme are scaled with the grid refinement. Modeled discontinuities become thinner with the spatial step decrement, but the width of the smeared discontinuity expressed in number of spatial steps remains constant. This effect is illustrated in Fig. 33a, where the numerical solution of the test problem in the vicinity of the jump in the exact solution is shown for various numbers of spatial steps. The effect of the grid refinement in the vicinity of weak discontinuities of the exact solution is somewhat different – Fig. 33b. The solution in the whole region of the rarefaction wave is smeared. However, with the grid refinement the numerical solution becomes closer to the exact one. If we look at points joined by the thick solid line, we can see that the numerical solution tends towards the right position of the weak discontinuity.

4. Inhomogeneous velocity field independent on the solution

Considering advection in inhomogeneous velocity field independent on the solution we should consider two cases. In the first case the solution u has a sense of a density function. The advection equation in the conservative form should be used

$$u_t + [a(x,t)u]_x = 0. \tag{61}$$

However, if u has a sense of information (eg. number identifying material, internal state variable) the nonconservative form should be used

$$u_t + a(x,t)u_x = 0. \tag{62}$$

It is obvious that for the both cases the scheme should have a different form. In the case of Eq. (61) we can make use of the algorithm (60). In the corrector step we can determine the flux by

$$F_{i+1/2}^{n+1/2} = a\left(x_i + \frac{h}{2}\,,\ t^n + \frac{\tau}{2}\right) u_{i+1/2}^{n+1/2}\,. \tag{63}$$

Figure 33 shows results of the solution of the square wave test (1.43) for Eq. (61). The velocity field includes a stationary jump at $x = 50$

$$a(x,t) = \begin{cases} 1 & \text{for } x \le 50; \\ 0.5 & \text{for } x > 50; \end{cases} \qquad x \in [0,100]\,. \tag{64}$$

The space step is $h = 1$ and the time step is taken half of the maximum accessible value. Results shown in Fig. 34 correspond to $t = 90$.

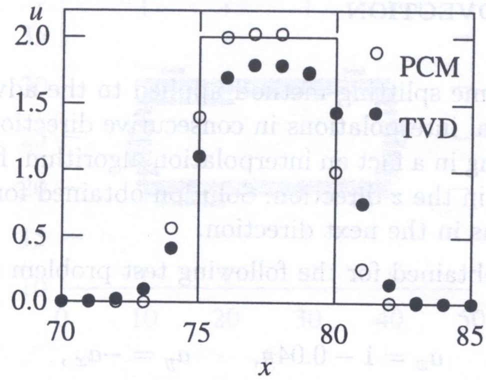

Fig. 34. Results of the square wave test of the conservative version of the PCM scheme and TVD scheme in the case of inhomogeneous, solution independent velocity field

The PCM scheme produces a small overshot. However, the solution is much closer to the exact solution than in the case of the TVD scheme.

In the case of the nonconservative advection equation the scheme should be nonconservative as well. It enables us to use the same value of velocity in calculation of $u_{i-1/2}^{n+1/2}$, $u_{i+1/2}^{n+1/2}$ and u_i^{n+1}. Therefore, the limitation algorithm preserves monotone profiles exactly. Let us observe, that $u_{i+1/2}^{n+1/2}$ values are different at the both sides of cell boundaries, because different velocity values are used for their determination. Hence, the corrector step has a form

$$u_i^{n+1} = u_i^n - m\nu \left(u_{i+1/2}^{n+1/2(L)} - u_{i-1/2}^{n+1/2(R)} \right), \qquad \nu = \lambda a, \tag{65}$$

where $u_{i+1/2}^{n+1/2(L)}$, $u_{i+1/2}^{n+1/2(R)}$ mean left and right values at the cell boundary. In the predictor step we can use the algorithm (48). The value of a should correspond to a mean value of the velocity along the characteristic coming to the node i at $t = t^{n+1}$. It can be determined in the following way. In the first step we use the PCM scheme with the algorithm (60) for the solution of Eq. (54). This way we determine an approximate value of the velocity at the starting point of the characteristic at $t = t^n$. Then we can take an average of this value and $a(x_i, t^{n+1})$ as a.

Figure 35 shows a result of the square wave test for Eq. (62). The velocity field is given by (64). As it could be expected, the scheme is perfectly monotone and produces very small smearing of the profile.

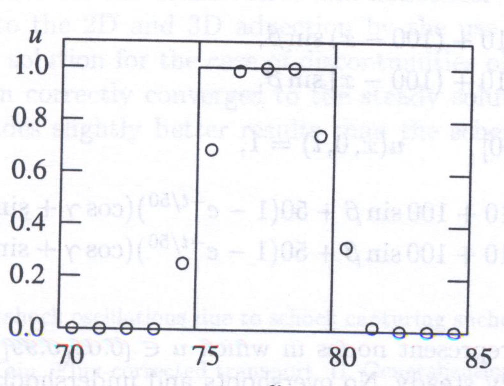

Fig. 35. Results of the square wave test of the nonconservative version of the PCM scheme in the case of inhomogeneous, solution independent velocity field

5. Multidimensional advection

As it was shown in [10], the time splitting method applied to the advection equation is equivalent to a sequence of onedimensional interpolations in consecutive directions. Therefore, we can use the described PCM algorithm, being in a fact an interpolation algorithm, first in the x direction, than in the y direction and eventually in the z direction. Solution obtained for a given direction constitutes the initial value for calculations in the next direction.

Figure 36 presents results obtained for the following test problem in 2D

$$\begin{gathered} u_t + (a_x u)_x + (a_y u)_y = 0, \qquad a_x = 1 - 0.04y, \qquad a_y = -a_x\,, \\ u(x,y,0) = \begin{cases} 1 & \text{for } (x,y) \in \Omega, \\ 0 & \text{for } (x,y) \notin \Omega, \end{cases} \qquad \Omega = \{x \in [10,40],\ y \in [20,30]\}, \\ x \in [0,50]\,, \qquad y \in [0,50]\,, \qquad u(x,0,t) = u(x,50,t) = u(0,y,t) = u(50,y,t) = 0. \end{gathered} \tag{66}$$

The problem is equivalent to a rotation of a slab of unit height around an axis crossing the center of the symmetry of the slab. Space steps in both directions are taken equal $h_x = h_y = 1$. The time step is chosen in such a way, that one revolution needs 600 time steps. In Fig. 36 points contained in the $[0.01, 0.99]$ range are shown. They mark the size of the smearing zone after one revolution. As we can see the thickness of the zone is very small. It means that the scheme behaves very well within the frame of the time splitting method.

In order to examine in deep properties of the PCM scheme, another test for 2D was performed. It is well known that a discontinuity front oblique with respect to the grid lines is difficult to treat by the advection algorithms. In the test problem given by (67), motion of such a discontinuity was modeled by the use of the PCM scheme. Another objective of the test was to check behaviour of the numerical solution, when the propagation velocity tends asymptotically to zero and the solution tends to the steady one. A spatially uniform but changing in time velocity field was assumed. The case $\beta = \gamma$ corresponds to the situation, when the velocity vector is normal to the discontinuity front. Otherwise, the discontinuity can be considered as an oblique one. Both cases were examined. In calculations, the same a value for the predictor and corrector steps was taken. The Courant number was accepted 0.5. Results of calculations are shown in Figs. 37 and 38.

$$\begin{gathered} u_t + a_x u_x + a_y u_y = 0, \qquad a_x = e^{-t/50} \sin\gamma > 0, \qquad a_y = e^{-t/50} \cos\gamma > 0, \\ u(x,y,0) = \begin{cases} 1 & \text{for } y \le 10 + (100 - x)\sin\beta, \\ 0 & \text{for } y > 10 + (100 - x)\sin\beta, \end{cases} \\ x \in [0,100]\,, \qquad y \in [0,100]\,, \qquad u(x,0,t) = 1, \\ u(0,y,t) = \begin{cases} 1 & \text{for } y \le 10 + 100\sin\beta + 50(1 - e^{-t/50})(\cos\gamma + \sin\gamma\tan\beta), \\ 0 & \text{for } y > 10 + 100\sin\beta + 50(1 - e^{-t/50})(\cos\gamma + \sin\gamma\tan\beta). \end{cases} \end{gathered} \tag{67}$$

Points in Figs. 37 and 38 represent nodes in which $u \in [0.01, 0.99]$ for the time $t = 500$, when the exact solution is practically steady. No overshoots and undershoots were detected. The steady positions of the discontinuities, shown by solid lines, agree well with the positions that can be concluded from the numerical solution. As in the 1D case, the width of the smeared discontinuities in the direction normal to their fronts is equal to approximately 3 spatial intervals. Seemingly large smearing in the x direction is only an effect of projection.

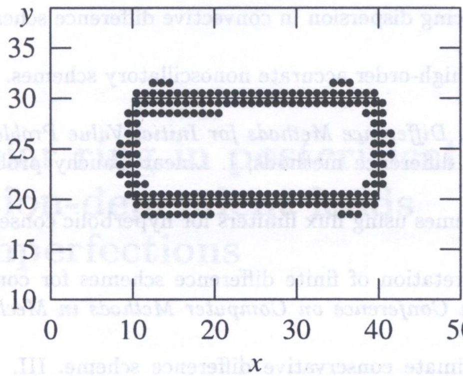

Fig. 36. Results of the rotating slab test for the PCM scheme; points correspond to the solution in the range [0.01,0.99]

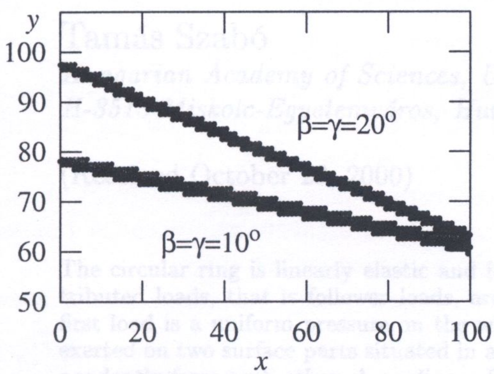

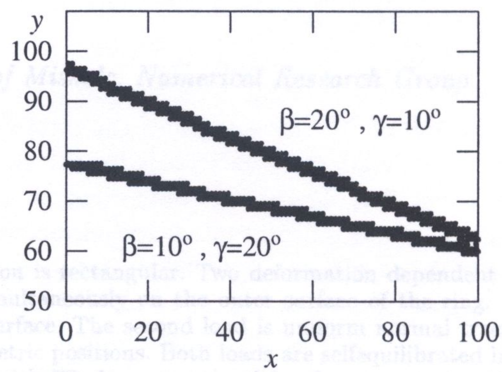

Fig. 37. Results of the oblique discontinuity test for the PCM scheme ($\gamma = \beta$); points correspond to the solution in the range [0.01,0.99]

Fig. 38. Results of the oblique discontinuity test for the PCM scheme ($\gamma \neq \beta$); points correspond to the solution in the range [0.01,0.99]

6. Conclusions

Results of performed tests have shown that the proposed scheme can be regarded as monotone. For the linear case the limiting algorithm preserve monotone profiles perfectly. In the nonlinear case small deviations from the monotone profiles can be expected. The scheme is easily generalized to the case of inhomogeneous velocity field independent on the solution. However, different forms of the algorithm should be used for the conservative and nonconservative advection equation. The scheme can be generalized to the 2D and 3D advection by the use of the time splitting method. The scheme provides proper solution for the case of discontinuities oblique with respect to the grid lines. The numerical solution correctly converges to the steady solution. Obtained results suggest that the PCM scheme provides slightly better results than the schemes considered to the date as giving the best results.

References

[1] M. Arora, P.L. Roe. On postshock oscillations due to schock capturing suchemes in unsteady flows. *J. Comput. Phys.*, **130**: 25–40, 1997.

[2] D.L. Book, J.P. Boris, K. Kain. Flux-corrected transport. II. Generalization of the method. *J. Comput. Phys.*, **18**: 248–283, 1975.

[3] S.Z. Burstein. Finite-difference calculations for hydrodynamic flows containing discontinuities. *J. Comput. Phys.*, **1**: 198–222, 1966.

[4] P. Collela, P.R. Woodward. The piecewise parabolic method (PPM) for gas-dynamical simulations. *J. Comput. Phys.*, **54**: 174–201, 1984.

[5] J.E. Fromm. A method for reducing dispersion in convective difference schemes. *J. Comput. Phys.*, **3**: 176–189, 1968.

[6] A. Harten, S. Osher. Uniformly high-order accurate nonoscillatory schemes. *SIAM J. Num. Anal.*, **24**: 279–309, 1987.

[7] R.D. Richtmeyer, K.W. Morton. *Difference Methods for Initial Value Problems.* Interscience, New York, 1967.

[8] W.G. Strang. Accurate partial difference methods, I. Linear Cauchy problems. *Arch. Rat. Mech.Anal.*, **12**: 392–402, 1963.

[9] P.K. Sweby. High resolution schemes using flux limiters for hyperbolic conservation laws. *SIAM J. Num. Anal.*, **21**: 995–1011, 1984.

[10] R. Trębiński. Geometric interpretation of finite difference schemes for convection transport equations in 2D and 3D. *Proc.of the XIII Polish Conference on Computer Methods in Mechanics*, 1307–1314, Poznan, Poland, 1997.

[11] B. Van Leer. Towards the ultimate conservative difference scheme. III. Upstream-centered finite-difference schemes for ideal compressible flow. *J. Comput. Phys.*, **23**: 263–275, 1977.

[12] H.Q. Young, A.J. Przekwas. A comparative study of advanced shock-capturing schemes applied to Burger's equation. *J. Comput. Phys.*, **102**: 139–159, 1992.